11th International Symposium on Turbulence and Shear Flow Phenomena (TSFP11)
Southampton, UK, July 30 to August 2, 2019

COHERENT STRUCTURES AND HEAT TRANSFER IN IMPINGING JETS WITH SWIRL

Sergey Abdurakipov

Kutateladze Institute of Thermophysics
Siberian Branch of the Russian Academy of Sciences
1 Lavrentyev Avenue, Novosibirsk, Russia
s.s.abdurakipov@gmail.com

Dmitriy Sharaborin

Kutateladze Institute of Thermophysics
Siberian Branch of the Russian Academy of Sciences
1 Lavrentyev Avenue, Novosibirsk, Russia
sharaborin.d@gmail.com

Dmitriy Markovich

Kutateladze Institute of Thermophysics
Siberian Branch of the Russian Academy of Sciences
1 Lavrentyev Avenue, Novosibirsk, Russia
dmark@itp.nsc.ru

Vladimir Dulin

Kutateladze Institute of Thermophysics
Siberian Branch of the Russian Academy of Sciences
1 Lavrentyev Avenue, Novosibirsk, Russia
vmd@itp.nsc.ru

ABSTRACT

In the present paper we report on the experimental study of coherent structures effect on convective heat transfer from a flat surface by an impinging jet with different swirl. The velocity fields were measured by using a time-resolved stereoscopic particle image velocimetry (PIV) system. Simultaneously, the impingement surface temperature was monitored via high-speed IR imaging. The distance H between the nozzle and impingement surface was fixed as one or two nozzle diameters. The Reynolds number was 5 000. Three cases of jet swirl rate were considered, viz., a non-swirling jet, low-swirl jet and high-swirl jet. In the latter case the flow was featured by a bubble-type vortex breakdown with central recirculation zone both for free and impinging jet configurations. Strong coherent velocity fluctuations, corresponded to large-scale vortex structures, were found for these flows. Besides, rotating coherent structures with azimuthal mode $|m| = 1$ are detected in fluctuations of the wall temperature for the impinging jets with high-swirl.

INTRODUCTION

Jet flows, impinging on flat surfaces, are relevant for a number of technical applications, including cooling and heating, coating, etc. Some of the applications require uniform heat and mass transfer. Others demand achievement of the highest possible local transfer rates. As one of the options, organization of impinging jets with swirl increases radial and tangential velocity components, causes broadening of the jet and enhances local convective heat transfer from the impinging surface. On the other hand, jet swirl may result in formation of stagnation zones with local flow recirculation which reduce overall heat transfer.

Huang and El-Genk (1998) have studied effect of the flow swirl on heat transfer from impinging surface and shown that it significantly affects the local heat transfer. The measurements of heat transfer were reported but the flow structure analysis was limited by visualization. Azevedo et al. (1997) have investigated effect of the flow swirl on the distribution of mass transfer coefficient for impinging jet with the Reynolds number in the range from 9 000 to 45 000 by using method of naphthalene sublimation. For the separation distances between the wall and nozzle of 2-8 diameters, they have found reduction of the mass transfer with increase of the swirl rate. Volchkov et al. (1996) have also outlined a reduction of the heat transfer from the surface with increase of the swirl for the distances of several nozzle diameters. However, for distances less than two nozzle diameters the flow swirl sufficiently increased heat transfer.

Abrantes and Azevedo (2006) have conducted velocity measurements in a swirling impinging jet at Re = 21 000 by using PIV and laser Doppler anemometry. The have confirmed that the flow swirl can significantly increase heat transfer from the surface for small separation distances (viz., for quarter of the nozzle diameter). Nozaki et al. (2003) have analyzed convective heat transfer in the wall region of a swirling impinging jet at Re = 4 000 for separation distance between the nozzle and wall of two nozzle diameters. The authors have combined PIV with PLIF (planar laser-induced fluorescence) method for the simultaneous measurements of the instantaneous velocity and temperature fields in the turbulent flow. They have shown that formation of the central recirculation zone in impinging jet with swirl reduces heat transfer from the wall surface.

It is important that swirling jets are often featured by unsteady flow dynamics, corresponding to precession of the jet's vortex core, which becomes very intensive in turbulent jets with strong swirl and vortex breakdown. This unsteady flow feature in impinging swirling jets is studied insufficiently, especially its contribution to the heat transfer. IR imaging is an efficient technique to perform wall temperature measurements for this purpose with sufficient spatial and temporal resolution (Carlomagno and Cardone, 2010). In particular, IR thermometry was successful used for the temperature measurements in swirling impinging jets by Ianiro and Cardone (2011).

The aim of the present paper is to investigate flow structure and dynamics of impinging jets with superimposed swirl by using the stereoscopic PIV technique and analyze coherent fluctuations of the wall temperature by IR imaging.

EXPERIMENTAL SETUP

The experimental setup corresponded to a closed hydrodynamic circuit, included a plexiglass test section, pump, overflow tank, piping system with flow meter and thermostat. Temperature of the circulating water was monitored by thermal resistance transducers, installed in the test section and water tank. During the experiments, the temperature of the water was kept constant at 25° C with the accuracy of 0.2° C. The jet

flow, organized by a contraction nozzle (with the outlet diameter of d = 15 mm), impinged normally on a flat heated surface made of a sapphire glass (4 mm thick, 150×150 mm in size). The Reynolds number, defined on the basis of the jets's bulk velocity, nozzle exit diameter and kinematic viscosity of the fluid, was fixed as Re = $U_0 d/\nu$ = 5 000. From the water side the sapphire glass was coated by a thin conductive film (1.2 μm thick) of indium-tin oxide (ITO, solid phase $(In_2O_2)_{0.9}$-$(SnO_2)_{0.1}$) transparent in the visible range. An electric current of 16 A passed through the coating, provided a uniform heating of 3.6 W/cm^2. The Titanium HD 570M (FLIR Systems ATS) IR-camera with a spectral range of 3.7-4.8 μm recorded the temperature of the conductive film on the heating element, which varied from 27° C to 38° C.

A vane swirler was mounted inside nozzle to produce jet with angular momentum (as in Alekseenko et al., 2007). Using swirlers with different inclination angles of the vanes, jets with different swirl rates (defined as the ratio of the jet angular momentum flux to the axial momentum flux, normalized by the nozzle exit radius) were produced. The swirl rates were estimated based on the geometrical parameters of the swirlers (Gupta et al., 1984):

$$S = \frac{2}{3}\left(\frac{1-\left(d_1/d_2\right)^3}{1-\left(d_1/d_2\right)^2}\right)\tan\left(\psi\right) \qquad (1)$$

Here d_1 = 7 mm is the diameter of the centerbody supporting the vanes, d_2 = 27 mm is the external diameter of the swirler, and ψ is the vanes inclination angle relatively to the axis. Swirlers with ψ = 30°and 55° provided the swirl rates of S = 0.41 and 1.0, respectively. The critical swirl rate for which a vortex breakdown occurred in a free jet flow configuration with formation of a recirculation zone was approximately 0.6.

The PIV system consisted of a Photonics DM high-repetition pulsed Nd:YAG laser (150 ns pulses with energy up to 8 mJ at a repetition rate of 10 kHz) and two Photon SA5 high-speed CMOS cameras (with 7.5 kHz rate of full frames with 1024×1024 pixel array and dynamic range of 12 bit), equipped with narrow band-pass filters with approximately 80% transmittance in the range of 532 ± 5 nm. 20-μm polyamide tracer particles with minimal buoyancy were added to the water to provide the PIV measurements.

DATA PROCESSING

An in-house "ActualFlow" software developed in the Institute of Thermophysics was used to acquire and process the PIV data. The cameras and laser were synchronized by a BNC 575 device from Berkeley Nucleonics. The acquisition rate was 3.5 kHz. Two independent runs were performed for each swirl case. 5500 images were recorded during each run. Spatial calibration of the PIV cameras was performed by using a planar calibration target (100×100 mm) and a third-order polynomial transforms (Soloff et al., 1997). The particle displacement was evaluated by using a multi-frame pyramid correlation algorithm (similar to that of Sciacchitano et al., 2012). Final size of the interrogation window was 16×16 pixels. The spatial overlap factor of the interrogation windows was set to 50%.

In order to analyze coherent structures in the flow, the velocity data sets were processed by a dynamic mode decomposition method (DMD, see Schmid, 2010). The decomposition provided a set of spatial basis functions $\boldsymbol{\phi}_n(\mathbf{x})$ with amplitudes $a_n(t_i)$ oscillating as complex Fourier harmonic $a_n(t_i) = \alpha_n \exp(\omega_n t_i)$, where ω_n are the complex values, with $\mathrm{Re}\omega_n$ representing the growth rate of the harmonic with frequency $\mathrm{Im}\omega_n$. Following the procedure of Jovanović et al. (2014), α_n describe amplitudes of the DMD modes ($\|\boldsymbol{\phi}_n\| = 1$).

$$\mathbf{u}\left(\mathbf{x},t_i\right) = \sum_{n=1}^{N} a_n\left(t_i\right)\boldsymbol{\phi}_n\left(\mathbf{x}\right) = \sum_{n=1}^{N} \alpha_n e^{\omega_n t_i}\boldsymbol{\phi}_n\left(\mathbf{x}\right) \qquad (2)$$

To reveal the effect of azimuthal hydrodynamics instability modes on the heat transfer, the measured wall temperature fields were processed by a discrete Fourier transform (3) with respect to the azimuthal angle θ.

$$\chi'_m\left(r,t_k\right) = \frac{1}{N_\theta}\sum_{j=1}^{N_\theta}\chi'\left(r,\theta_j,t_k\right)e^{-im\theta_j} \qquad (3)$$

Each 2D snapshot of the fluctuating temperature $\chi'(r, \theta, t_k)$ was decomposed into the complex Fourier amplitudes $\chi'_m(r, t_k)$. The snapshots were decomposed until the maximum wavenumber $|m|$ = 30. Note that since the analysed data were real, values of χ'_m for m = +1 and −1 were the complex conjugates. Principle component analysis was applied to the ensembles of the Fourier amplitudes via the singular value decomposition (SVD) to extract most intensive coherent structures in different azimuthal modes.

RESULTS

The mean velocity fields and wall temperature distributions for the impinging jets are shown in Figure 1. For the non-swirling jets, the velocity distributions at the nozzle exit are close to a "top-hat" profile. Downstream, the jets impinge normally on the flat surface and spread radially along the wall. The cooling appears to be the most efficient near the stagnation point. For the considered swirling jets, there is a central recirculation zone between the nozzle exit and wall. It is expected to be responsible for a local minimum of the cooling efficiency near the stagnation point due to small velocity magnitude near the wall. Besides, distributions of the surface temperature for the swirling jets are more sensitive to H/d change than for the non-swirling jets, since the wall location affects shape of the central recirculation zone.

Noteworthy, whereas central recirculation zone is not detected in free jet flows with the low-swirl S = 0.41 (e.g., Alekseenko et al., 2007), a conical recirculation zone is present for the impinging jets. Flows of both free and impinging jets with high swirl (S = 1.0) are featured by a breakdown of the vortex core and presence of a bubble-type central recirculation zone. In general, it is found that the high-swirl jet for H/d = 1 provides the most effective overall cooling of the impingement surface for the considered flow configurations. Also, intensity of the velocity fluctuations, including those induced by the flow precession, is the highest for this case.

Figure 2 demonstrates amplitudes of the DMD modes for the swirling impinging jets. The Strouhal number corresponds to the normalized frequency of the DMD modes: $\mathrm{St} = f_n d/U_0$, where $f_n = \mathrm{Im}\omega_n/2\pi$. There is a pronounced peak near $\mathrm{St} \approx 0.7$ for both H/d = 1 and 2 in the case of the high-swirl (S = 1.0). For the rest flow cases, amplitudes of the modes are considerably smaller and there are no pronounced peaks. This supports previous results that dynamics of high-swirl jets with

vortex breakdown is dominated by a global hydrodynamic instability mode (Oberleithner et al., 2011). Figure 3 shows the spatial distributions of the *x*-component of the turbulent kinetic energy and the most energetic DMD modes for the case $H/d = 1$. For the non-swirling and low-swirl jets, modes are shown for St = 0.52 and 0.48, respectively.

Vortex structures roll-up and grow in the mixing layer of the non-swirling jet. Downstream, they induce velocity fluctuations near the wall. For the swirling jets, the vortex structures are present both in the outer and inner mixing layers. Figure 3 demonstrates that intensity of the turbulent fluctuations increases with the swirl rate and exceeds 60% of U_0 for the high-swirl jet with vortex breakdown. Similar tendency is observed for the flows for $H/d = 2$ (the data is plotted in Figures 4 and 5). Previously, based on 2D PIV measurements and POD for turbulent free jets with high swirl and vortex breakdown, Oberleithner et al., (2011) and Alekseenko et al. (2012) have reported on a coherent structure, consisted of a precessing vortex core and secondary spiraling vortex. Later, based on time-resolved 3D PIV measurements by tomographic PIV, Alekseenko et al. (2018) have proven presence of such structure, which corresponded to the first azimuthal mode.

To analyze possible effect of such helical vortex structures on the heat transfer, 2D distributions of the temperature fluctuations of the impingement surface were decomposed into the azimuthal modes based on the Fourier transform. Figure 6 shows the radial distributions of the variances of the temperature fluctuations for the modes $m = \pm1, \pm2, \pm3$ and ±4 for the high-swirl jets. Near the stagnation point, the first mode has the highest amplitude both for $H/d = 1$ and 2. For $H/d = 1$, there is another region of intensive temperature fluctuations (for the considered modes) near $r/d = 2.5$.

To reveal coherent structures in different azimuthal modes, SVD has been applied for the Fourier amplitudes $\chi'_m(r, t_k)$ (similarly to the analysis of 2D pressure fields by Alekseenko et al., 2018). For example, Figure 7 shows the distributions of the first POD modes for $m = \pm1$ for the high-swirl impinging jets. According to the temporal coefficients of the SVD (not shown), the distributions correspond to rotating coherent structures with the highest amplitude of pulsations in the regions of $r/d < 1$ and $2 < r/d < 3$. One may expect that these oscillations are induced by helical vortex structures.

CONCLUSIONS

Unsteady flow dynamics and convective heat transfer in swirling impinging jet has been studied by combined application of time-resolved stereoscopic PIV and IR thermometry. For the considered separation distances between the nozzle and the flat impingement surface the cooling efficiency it found to be the highest for the jets with strong swirl, vortex breakdown and intensive flow precession. Dynamics of these flows is dominated by a coherent structure, consisted of large-scale vortex structures (similar to helical vortices detected in previous 3D PIV measurements for a free jet configuration). Besides, rotating coherent structures with azimuthal mode $|m| = 1$ are detected in for the wall temperature fluctuations for the high-swirl jets.

ACKNOWLEDGEMENTS

The research is supported by the Russian Science Foundation (grant No 16-19-10566).

REFERENCES

Abrantes, J.K., and Azevedo, L.F.A., 2006, "Fluid flow characteristics of a swirl jet impinging on a flat plate", *Proceedings, 13th International Symposium on Applications of Laser Techniques to Fluid Mechanics*, Lisbon, Portugal, pp. 26-29.

Alekseenko, S.V., Bilsky, A.V., Dulin, V.M., and Markovich, D.M., 2007, "Experimental study of an impinging jet with different swirl rates", *International Journal of Heat and Fluid Flow*, Vol. 28, pp. 1340-1359.

Alekseenko, S.V., Dulin, V.M., Kozorezov, Y.S., and Markovich, D.M., 2012, "Effect of high-amplitude forcing on turbulent combustion intensity and vortex core precession in a strongly swirling lifted propane/air flame", *Combustion Science and Technology*, Vol. 184, pp. 1862-1890.

Alekseenko, S.V., Abdurakipov, S.S., Hrebtov, M.Y., Tokarev, M.P., Dulin, V.M., Markovich, D.M., 2018, "Coherent structures in the near-field of swirling turbulent jets: A tomographic PIV study", *International Journal of Heat and Fluids Flow*, Vol. 70, pp. 363-379.

Azevedo, L.F.A., Almeida, J.A., and Duarte, L.G.C., 1997, "Mass transfer to swirling impinging jets", *Proceedings, 4th World Conference on Experimental Heat Transfer, Fluid Mechanics and Thermodynamics*, Brussels, Belgium, Vol. 3, pp. 1759-1766.

Carlomagno, G.M., Cardone, G., 2010, "Infrared thermography for convective heat transfer measurements", *Experiments in Fluids*, Vol. 49, No. 6, pp. 1187-1218.

Gupta, A.K., Lilley, D.G., and Syred, N., 1984, *Swirl Flows*. Abacus Press, Kent.

Huang, L., and El-Genk, M.S., 1998, "Heat transfer and flow visualization experiments of swirling, multi-channel, and conventional impinging jets", *International Journal of Heat and Mass Transfer*, Vol. 41, pp. 583-600.

Ianiro, A., and Cardone, G., 2012, "Heat transfer rate and uniformity in multichannel swirling impinging jets". *Applied Thermal Engineering*, Vol. 49, pp. 89-98.

Jovanović, M.R., Schmid, P.J., and Nichols, J.W., 2014, "Sparsity-promoting dynamic mode decomposition", *Physics of Fluids*, Vol. 26, No. 2, 024103 – 23 p

Nozaki, A., Igarashi, Y., and Hishida, K., 2003, "Heat transfer mechanism of a swirling impinging jet in a stagnation region", *Heat Transfer-Asian Research*, Vol. 32, pp. 663-673.

Oberleithner, K., Sieber, M., Nayeri, C.N., Paschereit, C.O., Petz, C., Hege, H.-C., Noack, B.R., and Wygnanski, I., 2011, "Three-dimensional coherent structures in a swirling jet undergoing vortex breakdown: Stability analysis and empirical mode construction", *Journal of Fluid Mechanics*, Vol. 679, pp. 383-414.

Schmid, P.J. 2010, "Dynamic mode decomposition of numerical and experimental data", *Journal of Fluid Mechanics*, Vol. 656, pp. 5-28.

Sciacchitano, A., Scarano, F., and Wieneke, B., 2012, "Multi-frame pyramid correlation for time-resolved PIV", *Experiments in Fluids*, Vol. 53, pp. 1087-1105.

Soloff, S.M., Adrian, R.J., and Liu, Z.C., 1997, "Distortion compensation for generalized stereoscopic particle image velocimetry", *Measurement Science and Technology*, Vol. 8, pp. 1441-1454.

Volchkov, E.P., Lukashov, V.V., and Semenov, S.V., 1996, "Heat transfer in an impact swirling jet", *Heat Transfer Research*, Vol. 27, pp. 14-24.

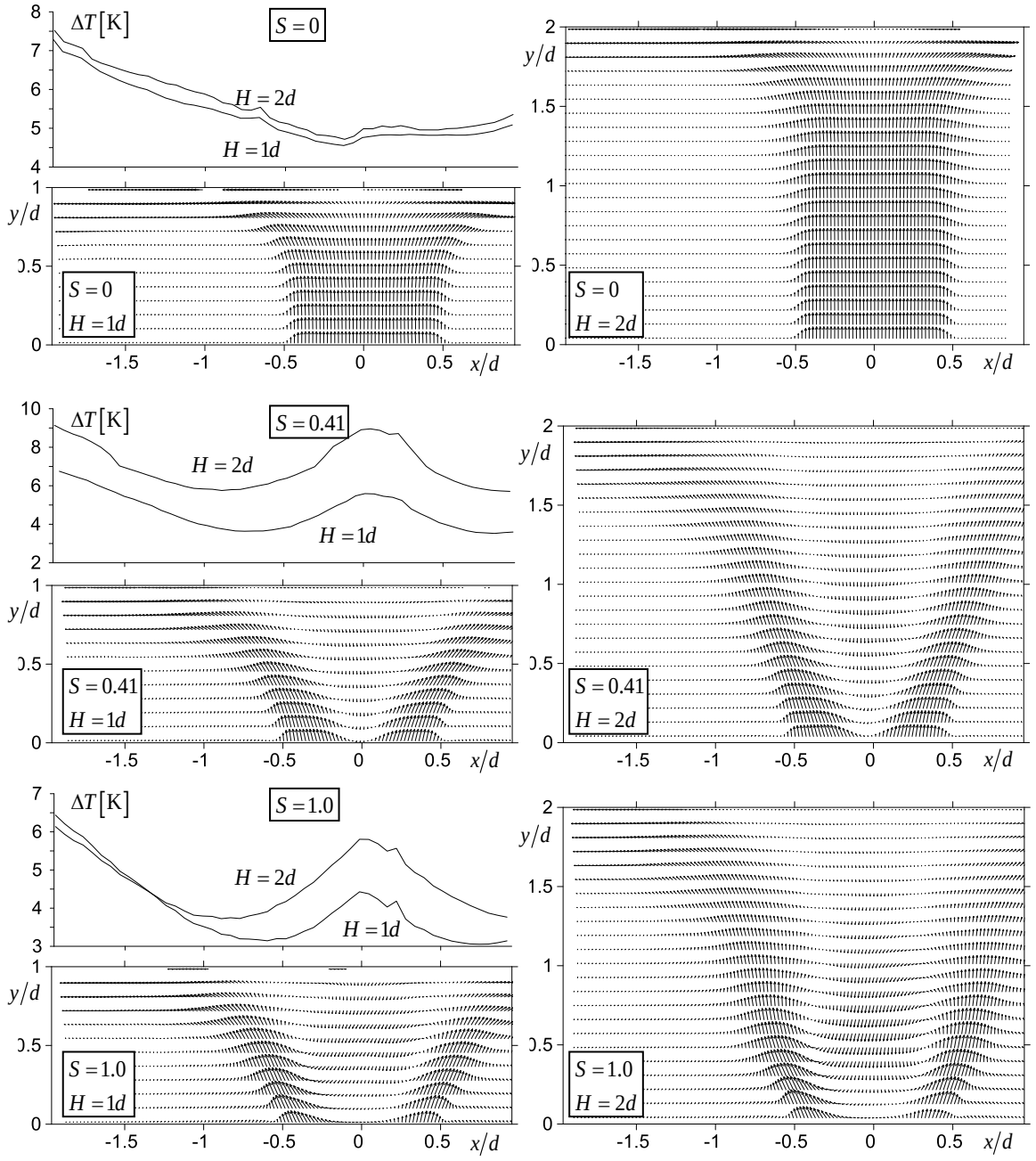

Figure 1. Time-averaged velocity field and wall temperature for impinging jets with different swirl rates

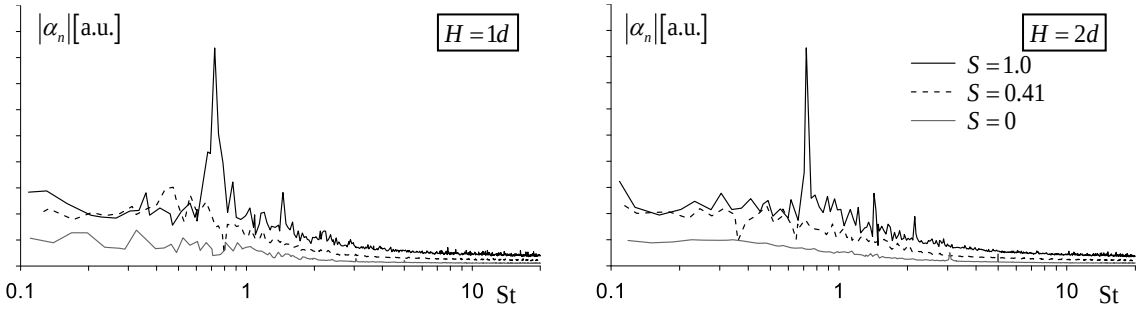

Figure 2. DMD spectra for impinging jets with different swirl rates

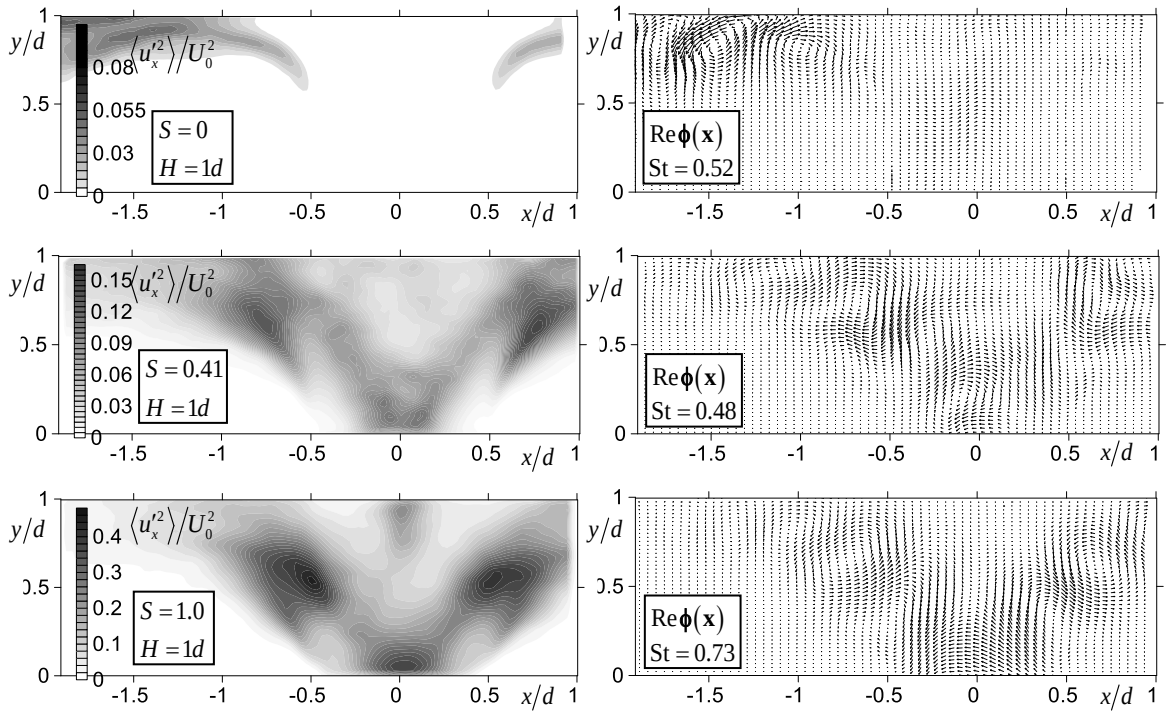

Figure 3. Spatial distributions of the *x*-component of the turbulent kinetic energy and the most energetic DMD modes (real part) for impinging jets with different swirl rates. $H/d = 1$

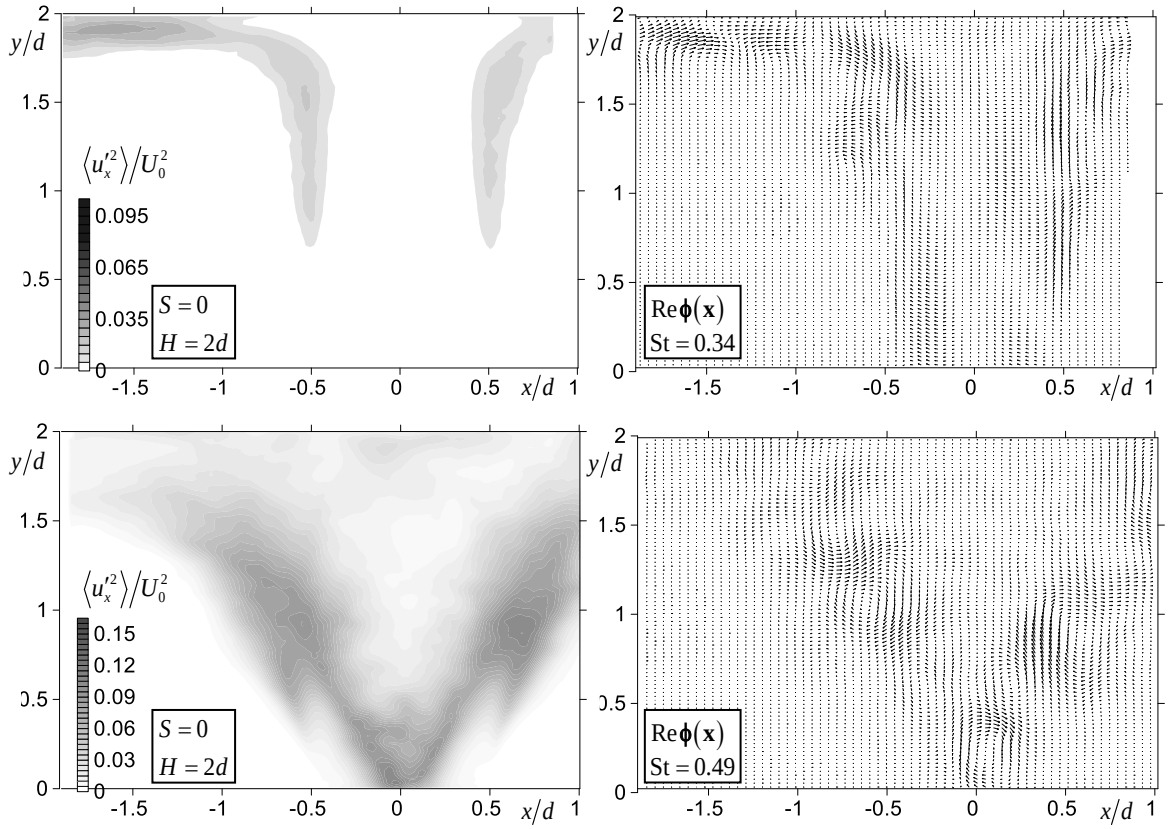

Figure 4. Spatial distributions of the *x*-component of the turbulent kinetic energy and the most energetic DMD modes (real part) for impinging jets with different swirl rates. $H/d = 2$

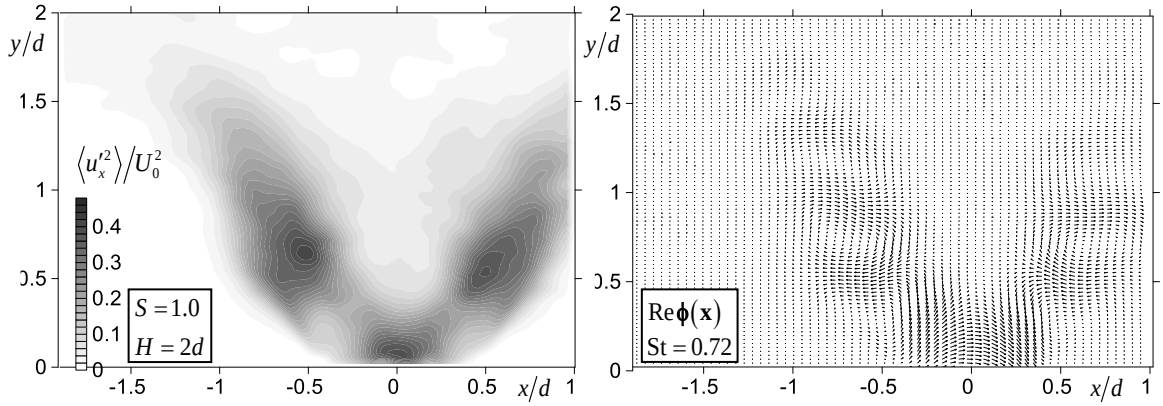

Figure 5. Spatial distributions of the *x*-component of the turbulent kinetic energy and the most energetic DMD mode (real part) for impinging jet with high swirl rate. $H/d = 2$

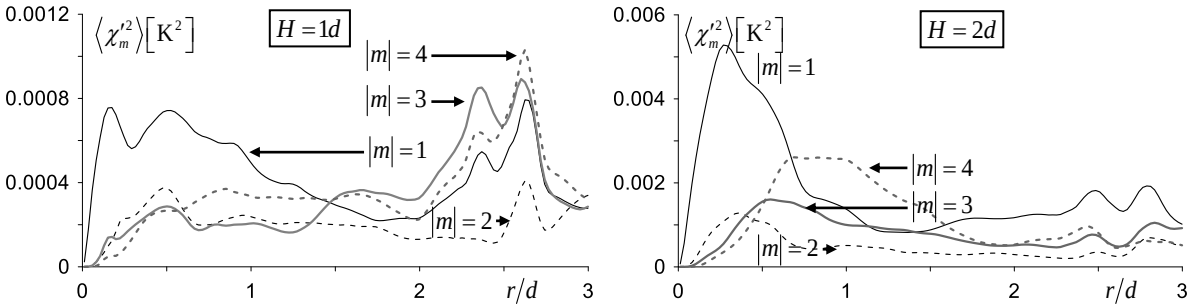

Figure 6. Squared amplitude of different azimuthal modes of the temperature fluctuations for impinging jets with high swirl rate ($S = 1.0$)

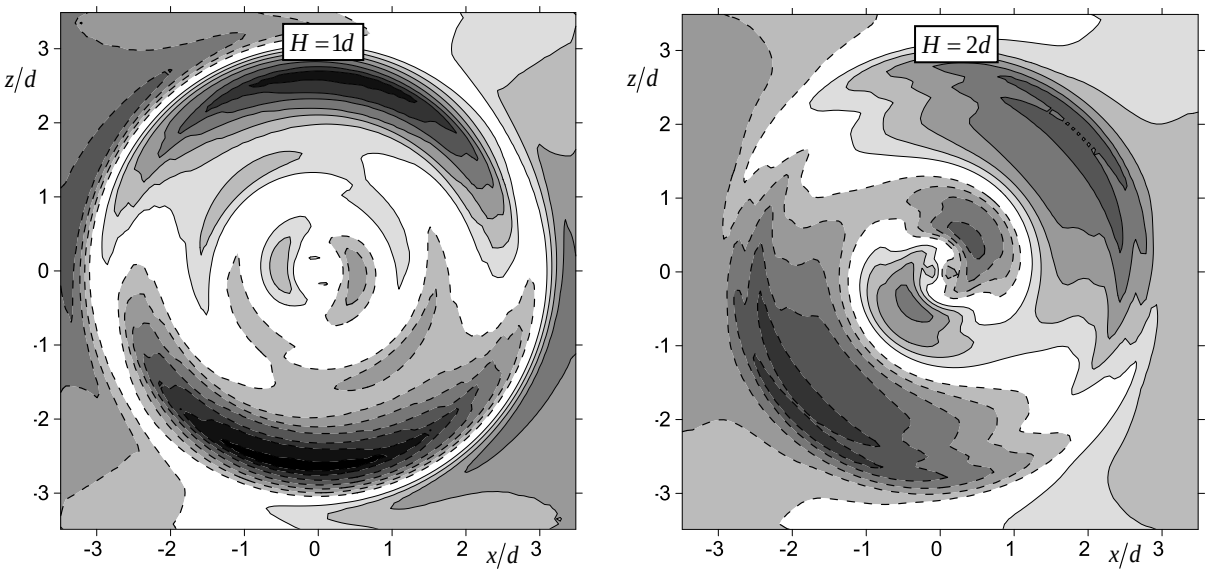

Figure 7. Coherent temperature fluctuations corresponding to the first POD mode (real part) of the first azimuthal mode ($|m| = 1$) for impinging jets with high swirl rate ($S = 1.0$). Solid and dashed lines correspond to levels of the positive and negative fluctuations, respectively